J Solid State Electrochem (2006) 10: 176–184
DOI 10.1007/s10008-005-0060-4

ORIGINAL PAPER

Elena Levi · Eli Lancry · Yossi Gofer · Doron Aurbach

The crystal structure of the inorganic surface films formed on Mg and Li intercalation compounds and the electrode performance

Received: 5 July 2005 / Accepted: 3 August 2005 / Published online: 13 September 2005

Abstract A crystallographic approach was applied to elucidate the influence of the nature of the surface films on the electrochemical behavior of Li and Mg intercalation compounds. This paper presents two examples: (1) protection of graphite electrodes by Li_2CO_3 surface films, and (2) the unique electrochemical behavior of Mg-containing Chevrel phases (MgCP) obtained by different synthetic routes. In the former case, the elucidation of the protection mechanism and the explanation of the high performance of such protected electrodes are based on the analysis of possible Li-ion motion in the carbonate crystal structure. In the latter case, a combination of synthesis, electrochemistry and XRD analysis was used to explain an unusual phenomenon: the difference between the excellent electrochemical behavior of the Chevrel phase (CP) based on Cu-leached $Cu_2Mo_6S_8$ (CuCP), and the poor electrochemical activity of the high-temperature synthesized MgCP, with the same phase composition. It is shown that this phenomenon is caused by MgO formation on the surface of the latter material. The different surface chemistry of the MgCPs obtained by the two different synthetic routes was substantiated by revealing the correlation between the electrochemical activity and the chemical stability of these materials under ambient atmosphere conditions.

Dedicated to Prof. Mikhail A. Vorotyntsev on the occasion of his 60th birthday.

E. Levi (✉) · E. Lancry · Y. Gofer · D. Aurbach
Department of Chemistry, Bar-Ilan University,
Ramat-Gan, Israel52900
E-mail: elenal@mail.biu.ac.il
Tel.: +972-3-5318954
Fax: +973-3-5351250

Introduction

It is well known that the composition of the films formed on the surface of Li insertion electrodes has a strong impact on their electrochemical behavior. For instance, the formation of a passivation layer comprising Li_2CO_3 on the surface of graphite electrodes prevents the co-intercalation of solution species, and the subsequent disintegration of the graphite particles [1]. It is well established that in order to obtain reversible intercalation and stable behavior, the surface films on insertion electrodes should be composed of materials that possess good ionic conductivity, so as to ensure fast ion transfer through the films. In general, for high ionic conductivity, the crystal structure of a material should meet certain requirements: [2].

1. Large number of mobile ions.
2. High concentration of empty sites available for ion transport.
3. Low activation barrier for the ion hopping.
4. Open channels for ion migration or diffusion.
5. Highly polarizable anionic framework.

We can find several examples of crystallographic approaches that deal with the mobility of Li^+ ions in different electrode materials, e.g., in the work of Ceder et al. [3–5]. However, the influence of the crystal structure of passivating surface films on the performance of insertion electrodes has not yet been presented in literature.

The general aim of the work was not to present new experimental results, but rather, based on existing data, to understand the correlation between the crystal structures of surface films formed on different insertion electrodes, their ionic conductivity, and their influence on the electrochemical behavior. In this work we present the crystallographic explanation for possible ionic transport within surface films comprising crystalline components. Such an approach cannot give quantitative parameters such as diffusion coefficients (that can be

obtained, for instance, by computer modeling). However, as shown previously, (e.g., in the classic Solid State Chemistry book by A. R. West or in the works of G. Ceder's group) only analysis of the ionic motion in crystal structure could explain the mechanism of different ionic mobility in solids. An enormous advantage of such crystallographic analysis is that it does not need the use of complicated methods, but can be done simply on the basis of the crystal structure geometry. Thus, our purpose was to demonstrate the effectiveness of this approach in cases of well-known components in surface films that cover electrode materials. We illustrate the above analysis for two materials: Li_2CO_3, as a good Li^+ conductor, and MgO, as a poor Mg^{2+} ion conductor. Furthermore, on the basis of the latter example, we explain the unusual electrochemical inactivity of MgCP obtained by high-temperature synthesis (new experimental data).

Experimental section

Chevrel phases with the intended $A_XMo_6S_8$ (A = Cu, Mg) composition were synthesized by high temperature, solid-state reaction of the powdered elements mixture in evacuated (10^{-3} Torr), sealed quartz tubes. In the case of MgCP, in order to prevent the reaction of Mg with the quartz, the mixture was contained within a corundum crucible, located in the sealed quartz ampoule. The heating procedure consisted of four sequential stages: (1) heating at 450 °C for 24 h; (2) heating at 700 °C for 24 h; (3) heating at 1,050 °C for 48 h; (4) cooling down to room temperature at the rate of 120 °C/h.

The synthetic products thus obtained were leached in order to remove the ternary metal under ambient air atmosphere in either 6 M HCl in water, or in 0.2 M I_2 in acetonitrile (AN), according to the procedures described previously [6]. After leaching, the powders were filtered with a fine glass frit, washed with the same solvent, and dried in an oven at 120 °C. In the case of MgCP, the as-synthesized product was also tested electrochemically.

The electrochemical behavior (galvanostatic cycling) of the leached materials was studied in standard three-electrode cells at a current density of 0.1 mA cm^{-2} using a computerized Arbin Inc. (USA) multichannel battery tester. Composite cathodes were prepared with 80% active mass, 10% carbon black, and 10% PVdF pasted on stainless steel mesh (mass load ca. 10 mg/cm^2). Strips of Mg foil served as counter and reference electrodes. Electrolyte solutions comprising 0.25 M $Mg(AlCl_2BuEt)_2$ in THF (DCC/THF) were used. Both Mg and $Mg_XMo_6S_8$ electrodes behave reversibly in these solutions [8].

The XRD studies were performed with a Bruker Inc. (Germany) AXS D8 ADVANCE diffractometer (Cu Kα radiation). For air-sensitive compounds, the samples were loaded in the Ar-filled glove box, and were protected from air by Mylar films.

Results and discussion

Ionic conductivity and crystal structure relations: Li_2CO_3 and MgO

Li_2CO_3

The crystal structure of this compound is well established [9]. Nonetheless, its effect on Li ionic conductivity is not discussed in the literature, despite its enormous importance and its ubiquitous existence as a component of lithium passivating surface films on lithium and lithiated graphite electrodes [10].

In order to understand the implications of the crystal structure on its Li ionic conductivity, the crystal structure of Li_2CO_3 should be examined in detail. Figure 1a illustrates a layer consisting of separate planar $CO_3^=$ groups, coordinated by Li^+ ions. Figure 1b demonstrates the alternating stacking of the planar $CO_3^=$ groups that resembles a chessboard. Note that the layers shown in Fig. 1a are perpendicular to the image plane in Fig. 1b. The $CO_3^=$ groups have different orientations in the columns, located one above the other. As a result, the unit cell parameter that is perpendicular to the $CO_3^=$ plane is four times bigger than the distance between the layers.

The Li^+ ions are located in tetrahedral sites in this crystal structure. The space distribution of the tetrahedra [LiO_4] is anisotropic: they form layers with a relatively compact package. Figure 1c shows the polyhedral representation of one of such layers with pairs of the edge-sharing [LiO_4] tetrahedra, which can be regarded as structural units. Each pair is connected with four other units in the same layer and two units from adjacent layers. In addition, every oxygen ion in the corner of the [LiO_4] tetrahedra is bonded to one carbon atom. Figure 1d displays the same structure from a different angle that reveals the linkage of two adjacent layers of [LiO_4] tetrahedra. As can be seen, the atomic density between the layers is much lower than within the layers. Thus, in spite of the three-dimensional linkage of the [LiO_4] tetrahedra, the Li^+ ion motion is expected to be restricted by the diffusion within the layers.

In ionic conductors, the conductivity mechanisms involve ionic hopping from site to site as critical steps. Thus, in the case of Li_2CO_3, the most important feature of the crystal structure for high ionic conductivity is the linkage of the [LiO_4] tetrahedra in the layer. The distances between adjacent Li ions in the layer for the edge-sharing and corner-sharing [LiO_4] tetrahedra are equal to 2.70 and 2.98 Å, respectively, which is the regular distance between cations in the ionic compounds. However, the energetic barriers for Li^+ hopping decrease considerably due to the presence of empty tetrahedral sites, which serve as transport sites for Li diffusion (Fig. 1e). Thus, high Li conductivity in Li_2CO_3 results from the alternation of the occupied (by Li^+) and empty oxygen tetrahedra linked by common faces. This

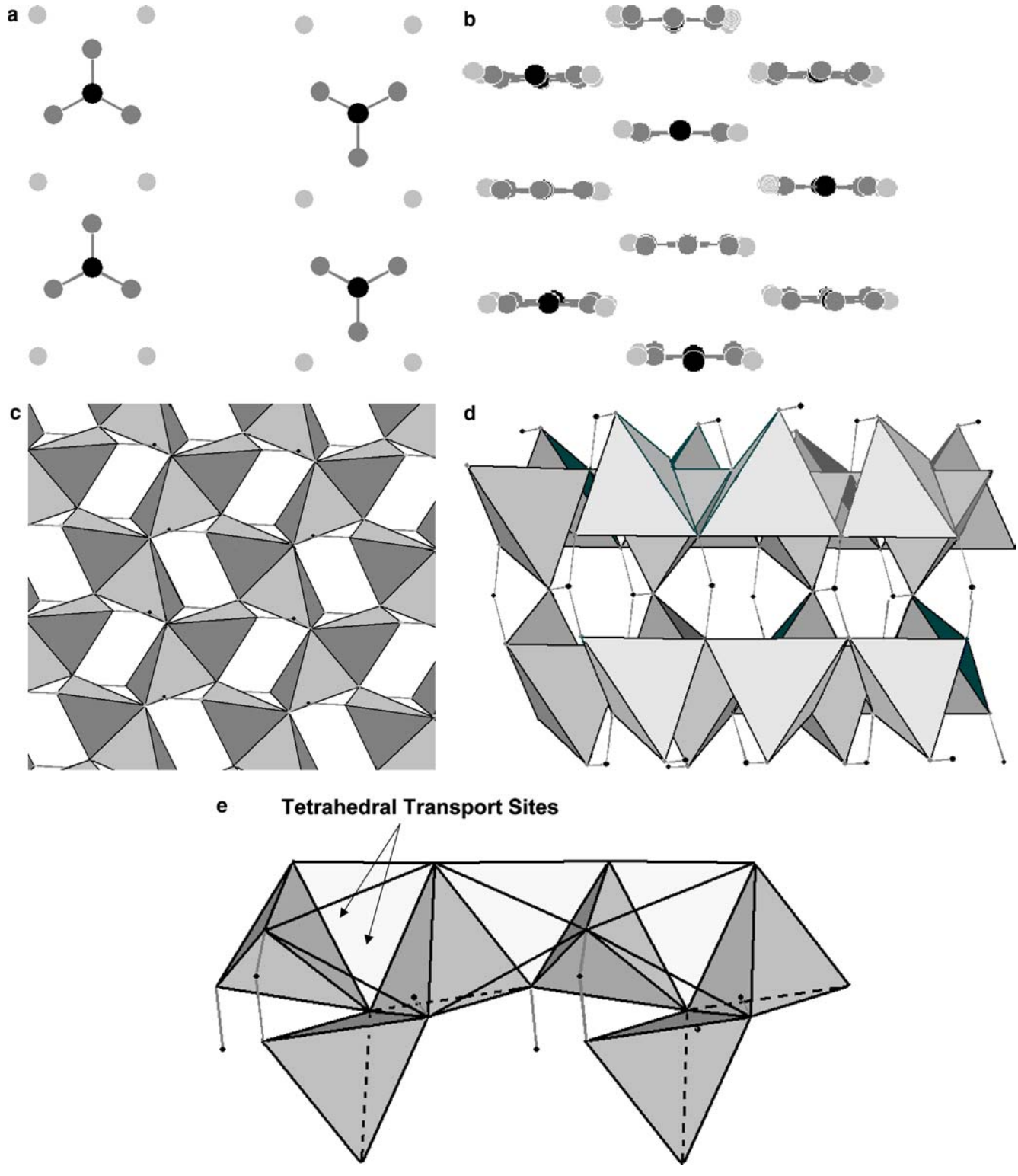

Fig. 1 The crystal structure of Li_2CO_3: **a** A single layer of the planar $CO_3^{=}$ groups, coordinated by Li^+ ions (carbon atoms are *black*, oxygen atoms are *taupe*, lithium ions are *light gray*). **b** A stacking of the layers described in (Fig. 1a). **c** A layer of the linked [LiO_4] tetrahedra. **d** A linkage of two layers described in (Fig. 1c). **e** Transport sites

means that the Li_2CO_3 formation on the surface of lithium metal or graphite particles does not block the transport of Li ions to and from the active mass, rendering it available for electrochemical activity. In addition, in contrast to graphite, the penetration of electrolyte-coordinated Li^+ ions through the crystal of Li_2CO_3 is not possible, as this structure does not contain penetrable, weakly bonded, Van-der Waals gaps. Thus,

the formation of Li_2CO_3-based passivation films on lithium metal or graphite electrodes may play a very positive role in their stabilization in Li battery electrolyte solutions.

MgO (or LiF)

MgO has a NaCl type crystal structure. The diffusion of ions within this structure was described in detail (ref. 2, p. 301). In spite of the relatively short distance, of 2.98 Å between adjacent Mg^{2+} ions and the edge-sharing linkage of the [MgO_6] octahedra, the Mg^{2+} ion motion in the *ideal* crystal structure is impossible due to the full occupancy of the octahedral sites. As a result, the only possible mechanism for ion mobility in this crystal structure relies on vacancies, but even the latter is problematic for the case of Mg^{2+} ions, due to their divalent character, resulting in high energetic barriers for the cation hopping. Hence, the formation of MgO, covering the surface of the electrode mass, is expected to inhibit its electrochemical activity. Since MgO is both an electronic and an ionic insulator, the term "passivation", mentioned so many times in connection with the solid electrolyte interface (SEI) layers on lithium or lithium intercalation compounds, is an adequate description for the case of magnesium. Likewise, a similar effect is observed when LiF, which possesses the same crystal structure, is formed and accumulated on the surface of Li or Li–graphite electrodes during their cycling in $LiPF_6$ or $LiBF_4$ containing solutions [11]. In this case, it can be observed that the impedance measured from cycled electrodes increases as the SEI layer is enriched with LiF.

The electrochemical activity of $Mg_XMo_6S_8$ obtained in different synthetic ways

Recently, it was shown that the pure Chevrel framework, Mo_6T_8 (T = S, Se), is a unique cathode material for secondary Mg batteries. In contrast to many other known intercalation compounds that show excellent activity with Li^+, but extremely poor activity with Mg^{2+} ions, Mo_6T_8 inserts 2 Mg^{2+} ions per formula unit [6–8, 12–18] reversibly and relatively rapid. Figure 2 shows typical first and sixth galvanostatic discharge curves for $Mg_XMo_6S_8$ obtained in different synthetic ways. Figure 2a is related to leached (empty) $Cu_2Mo_6S_8$ ($X = 0$ for $Mg_XMo_6S_8$). As can be seen, in the first Mg insertion, full theoretical capacity is reached, while in the subsequent cycles the capacity is stable, but lower, due to Mg trapping in the crystal structure of the Chevrel phase [14–16]. Previously, it was also shown that the Mg intercalation–deintercalation into Chevrel phases occurs via phase transition processes, including two stages:

$$Mo_6S_8 \rightarrow MgMo_6S_8 \rightarrow Mg_2Mo_6S_8 \quad [7]$$

As was suggested [6], the unique ability of these materials to insert polyvalent cations results from their

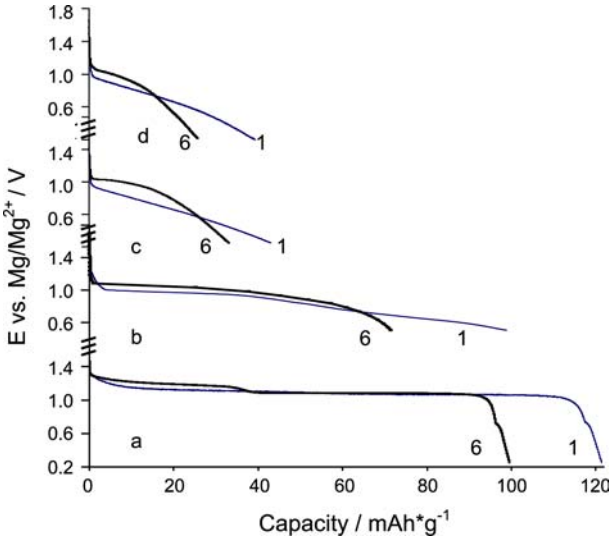

Fig. 2 The discharge capacity of different $Mg_XMo_6S_8$ in the first (*gray line*) and the sixth (*black line*) galvanostatic cycles (THF/0.25 $Mg(AlCl_2BuEt)_2$ solutions, C/10 rates, Mg counter electrodes): **a** I_2/AN or HCl/H_2O leached CuCP ($X = 0$). **b** I_2/AN leached MgCP ($X = 0$). **c** HCl/H_2O leached MgCP ($X = 0$). **d** As-prepared HT-MgCP ($X = 1.1$)

unusual crystal structure, based on metallically bonded octahedral Mo_6-clusters [19]. Of the two possible anions constituting the Chevrel phase structure, the selenide has a more polarizable anionic framework, and thus, exhibits a faster Mg insertion kinetics than the sulfide [17] . However, in practical battery terms, the specific capacity of the selenide is obviously lower, owing to its higher molecular weight. Incidentally, the sulfide, Mo_6S_8, which is more attractive as a practical cathode material, is thermodynamically unstable and can be synthesized only indirectly by chemical or electrochemical leaching of the more stable, ternary cation-containing Chevrel phases, e.g., CuCP. The leaching product obtained after Cu removal, i.e., empty, pure CP, shows excellent stability upon long-term cycling at C/10–C/5 rates, with a specific capacity of 90–105 mAh/g at room temperature [7].

Similar to CuCP, MgCP can be synthesized by direct HT synthesis (1,000–1,200 °C) from the elements or the sulfides [20]. Synthesizing and directly using MgCP as a cathode material for Mg batteries is appealing as it will considerably reduce the cost of the cathode materials. However, initial tests have revealed that MgCP obtained by direct HT synthesis shows poor electrochemical activity [6]. In previous work we only mentioned this fact, but the experimental results describing this phenomenon were presented in this work for the first time. Figure 2d presents the chronopotential response of the MgCP synthesized by direct HT synthesis. (Fig. 2b, c is discussed later) As can be seen, the capacity of the electrode material depends on the way of its preparation: the theoretical capacity of 122 mAh/g was obtained for Chevrel phase, produced by leaching of $Cu_2Mo_6S_8$ (Fig. 2a) and only one-third of the theoretical capacity

was obtained with $MgMo_6S_8$, the product of a direct solid-state synthesis (Fig. 2d). The reasons of such enormous difference might be the following:

1. A completely different phase composition of the *bulk* of the active material. For instance, MgCP formed in the solid-state reaction could have a different crystal structure than that of the product of the electrochemical reaction. Note that some small amount of the impurities in the bulk of the active mass cannot change the specific capacity of the material in such a dramatic way (The decrease in the capacity should be proportional to the amount of the impurity in most cases).
2. A completely different phase composition of the *surface films* is formed on the identical active material. In this case, even molecular layers of the surface films can change drastically the capacity of the electrode material, because the crystal structure of the surface films may not be favorable for ionic transport through the film.

The XRD analysis was performed in order to clarify the actual reason for the poor electrochemical activity of MgCP, as a product of the solid-state synthesis. Figure 3 presents the XRD pattern of the direct HT synthetic product (the exact stoichiometry was $Mg_{1.1}Mo_6S_8$) and that of the first-stage product, obtained by electrochemical intercalation ($MgMo_6S_8$). One can see that these diffraction patterns are identical, apart from the different intensity of the diffraction peaks at relatively small angles ($2\theta = 10/25°$), which results from the different experimental conditions for the XRD analysis: acquisition under open air for the HT synthetic product, and film-protected Mylar for the electrochemically synthesized material.

In order to confirm the identity of the host crystal structure in the case of CuCP and MgCP, metal extraction (leaching) was performed for both materials according to the same procedure. Figure 4 compares the XRD patterns of these leached products. One can see that the patterns are identical and they also match the literature-reported data for metal-free Mo_6S_8 (PDF 27-0319). Thus, the bulk structure of the active cathode mass does not depend on the synthetic route.

Figure 2b and c show the electrochemical responses of the Mo_6S_8 electrodes, whose active mass was obtained by leaching MgCP in two different procedures (see the Experimental section). The capacity of the material leached in I_2/AN (Fig. 2c) is identical to the pristine MgCP (Fig. 2d), while the material leached in HCl/H_2O (Fig. 2b) results in a much higher specific capacity, compared to the pristine MgCP. This correlation between the capacity and the leaching conditions of MgCP, obtained with the high temperature synthesis product, is in contrast to the electrochemical behavior of the leached CuCP [7]. For the latter, similar change in the leaching conditions from I_2/AN to HCl/H_2O did not affect the specific capacity obtained, that was equal to the theoretical one in the first discharge process. These results suggest that the difference in the electrochemical activity of the two materials is associated with surface properties, rather than with bulk ones. Moreover, they indicate that the MgCP surface is more sensitive to the leaching condition than that of CuCP.

According to the electrochemical and XRD results, we can propose:

1. The poor electrochemical activity of the HT-synthesized MgCP relates to the surface of the Chevrel phase rather than to its bulk.
2. The surface state of the HT-synthesized MgCP is different from that of CuCP (e.g., by surface films).

In order to study the difference between the surface of MgCP and CuCP, it is necessary to analyze all the data related to the surface state of these materials. Unfortunately, some commonly used surface sensitive techniques, such as XPS, were found to be inadequate for distinguishing between the various surface oxides that we assume to be responsible for this difference.

Previous studies revealed that the oxidation of CuCP during leaching leads initially to the formation of Mo oxides [21]. In fact, sometimes the XRD patterns of the

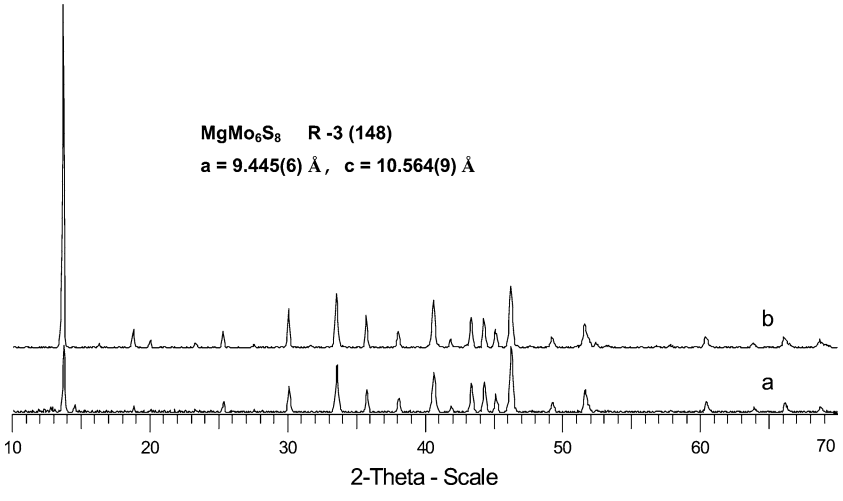

Fig. 3 The XRD patterns of MgCP obtained by different synthetic routes: **a** The first stage product of the electrochemical Mg intercalation into leached CuCP. **b** Product of the HT-synthesis with intended formula $Mg_{1.1}Mo_6S_8$

leached CuCP show the presence of MoO_2 (Fig. 5a). Note that the latter cannot be detected in the XRD patterns of the initial (before leaching) CuCP due to superposition of the diffraction peaks. However, electrochemical measurements showed that the presence of a small amount of molybdenum oxide is not detrimental to the Chevrel phase activity with magnesium. In order to explain why the presence of MoO_2 on the surface of CuCP does not hamper the Mg^{2+} intercalation, it is necessary to re-examine the crystal structure of this oxide [9]. MoO_2 has a crystal structure similar to that of rutile, with one-dimensional channels comprised of empty cationic sites, which are available for cation hopping. As a result, MoO_2-comprising surface films that may be formed on CuCP upon synthesis and leaching are not detrimental to the electrochemical activity of the material in Mg batteries, because MoO_2 does not block the transport of Mg^{2+} ions through the oxide layer into the bulk of the electrode particles.

In the case of MgCP, the material's oxidation results in the formation of the very stable MgO, sometimes in an amount that can be clearly detected by XRD analysis (Fig. 5b). As was discussed above, Mg^{2+} ion transport in the latter compound is impossible. Thus, even a thin MgO film formation on the surface of the CP can explain the poor electrochemical activity of MgCP. The electrochemical behavior of the leached MgCP depends on the reaction of this Mg^{2+} -nonconducting film with the solvent upon leaching. The electrochemical results (Fig. 2b, c) indicate, as expected, that leaching in I_2/AN does not change the structure of the MgO film, while leaching in HCl/H_2O results in the partial removal of the film, and, consequently, activation of the material.

The chemical stability of $Mg_XMo_6S_8$ obtained in different synthetic ways

It is clear that ionic conduction through surface films should be symmetrical, for Mg insertion as well as for Mg removal. Thus, passivation films, which prevent Mg transport into the material bulk, should also inhibit its extraction. The Mg-containing Chevrel phase is a reducing agent, and is expected to be sensitive to atmospheric oxygen and water. The reaction of water or oxygen with Chevrel phases containing another metallic element (Cu, Mg), is followed by the elevation of the oxidation state of the molybdenum and the extraction of the second metal. This reaction necessitates the transfer of the metal ions from the bulk material, through the material/air interface, in a similar manner to electrochemical deintercalation. The rate of this stage of the reaction, i.e., the chemical stability of the material under atmospheric condition, should be related to the degree of the electrochemical activity, when both of them are dominated by surface films. Thus, we are looking for a correlation between the electrochemical activity of MgCP prepared in various ways and its atmospheric stability.

Figure 6 presents the changes in the XRD patterns of a Chevrel phase electrode (leached CuCP) in the fully intercalated state ($Mg_2Mo_6S_8$), over time. The sample was drawn out of the solution, rinsed with dry, pure THF, dried and mounted on a sample holder covered by a Mylar film under Ar atmosphere in a glove box. The sample was analyzed by XRD immediately, and after 3 days of storage under Mylar film. Since this sample was prepared as a composite electrode, the presence of the binder is expected to provide some protection for the material against reaction with air. As can be seen, the process can be ascribed to the rapid self-deintercalation:

$$Mg_2Mo_6S_8 \rightarrow MgMo_6S_8 \rightarrow Mo_6S_8.$$

It is not clear what is the oxidation agent that drives this demagnesiation process, as well as where the Mg goes. XRD analysis does not answer these questions, possibly due to the small amount and poor crystallinity of the new phases that form. A similar partial deintercalation was found for fully intercalated electrodes that

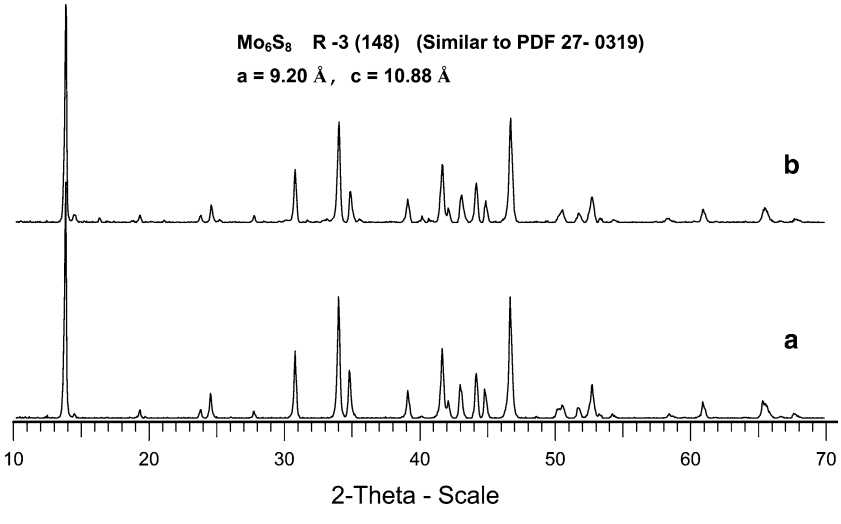

Fig. 4 The XRD patterns of the Chevrel host obtained by different synthetic routes: **a** Leached CuCP (leaching in HCl/H_2O). **b** Leached MgCP (leaching in HCl/H_2O)

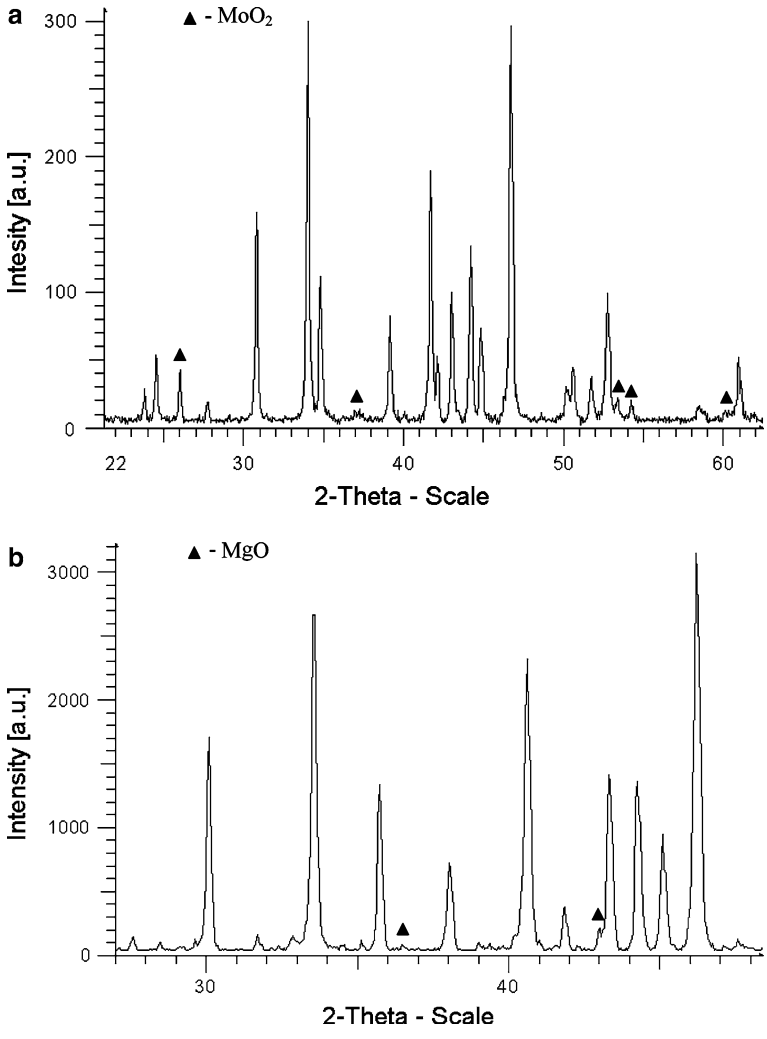

Fig. 5 The XRD patterns of the products oxidized in air: **a** Leached CuCP (leaching in HCl/H_2O). **b** HT-synthesized MgCP

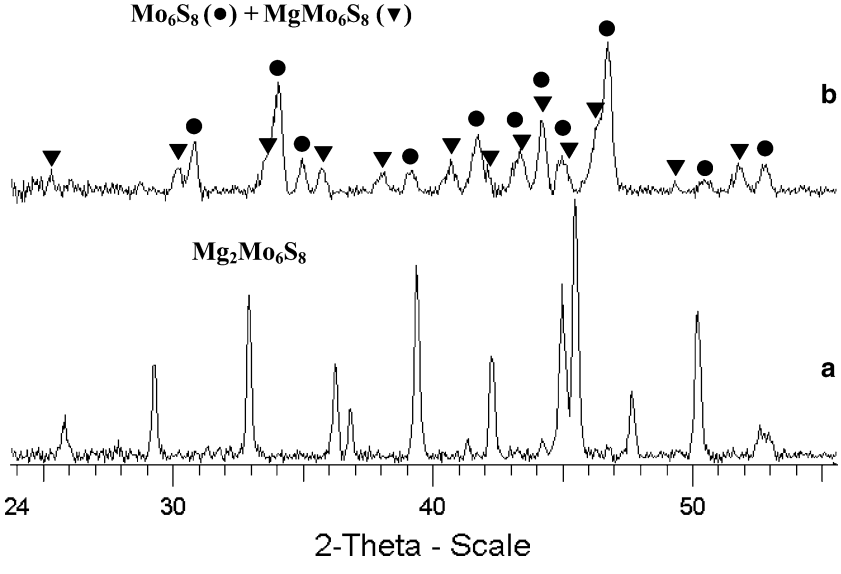

Fig. 6 XRD patterns (Mylar film protection) of a fully intercalated electrode based on the leached CuCP: **a** The measurements were performed immediately after electrochemical magnesiation. **b** The same electrode after 3 days of storage under Mylar film protection

were stored under Ar atmosphere in a glove box during several hours. In this case, the XRD analysis showed a mixture of $Mg_2Mo_6S_8$ and $MgMo_6S_8$, instead of pure $Mg_2Mo_6S_8$. It seems that the fully intercalated material reacts with the solvent molecules that are present in the glove box atmosphere, as well as with trace oxygen.

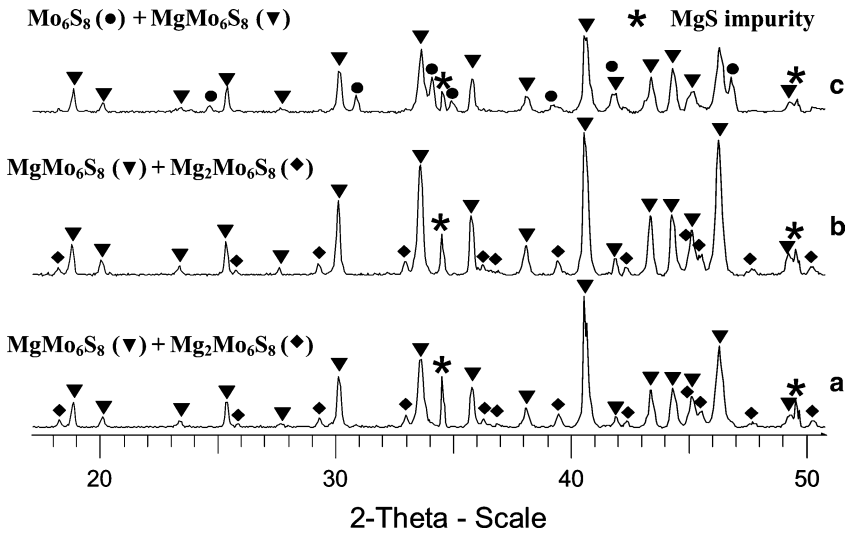

Fig. 7 XRD patterns of the HT-synthesized MgCP exposed to air: **a** After synthesis. **b** After 2 years of storage under dry air atmosphere. **c** After 2 years of storage under ambient (wet) air atmosphere

In the case of the XRD measurements of the samples protected by Mylar windows, we cannot exclude the possibility of oxygen diffusion through the Mylar film. As a result, in addition to the reaction of MgCP with trace organic contaminants (e.g., solvents, vapor) in the glove box, an amount of MgO is expected to be formed on the surface of the Chevrel phase particles, due to reaction with trace oxygen. In any case, it seems that such a film formed under a low concentration of oxygen in the atmosphere is not dense enough to block the transport of Mg ions outside. Hence, in line with the high electrochemical activity of the leached CuCP, the magnesium intercalated material shows high susceptibility towards spontaneous deintercalation when exposed from solution. Both characteristics can be explained by the absence of a compact passivation Mg oxide on the Chevrel phase particles.

All our attempts to synthesize a single phase $Mg_2Mo_6S_8$ were unsuccessful: the XRD analysis of the synthetic products always revealed a mixture of $Mg_2Mo_6S_8$ and $MgMo_6S_8$, sometimes with MgS as an impurity. The process is very similar to the self-demagnesiation of the fully intercalated electrodes in the glove box. Due to the inevitable exposure of the HT-synthesized MgCP to a trace of active atmospheric contaminants, its partial self-demagnesiation is inevitable, even under Ar glove-box conditions. The surface films, which are the product of demagnesiation under these conditions, do not block this partial reaction because they are not sufficiently passivating. However, once exposed to air (high oxygen concentration), MgCP demagnesiates via a formation of the compact passivation film that stops further material disintegration. Figure 7 presents the XRD patterns of the HT-synthesized MgCP: (a) material after synthesis, acquired under air conditions, (b) the same material after 2 years of storage under a dry air atmosphere. As can be seen, there is no discernable change in the phase composition of the synthetic product after prolonged storage.

Obviously, storage under a humid air atmosphere showed different results from storage under dry-air conditions (Fig. 7c), because in the former case, the MgO film on the surface may transform to brucite, $Mg(OH)_2$ with a layered crystal structure [9], which may transport Mg^{2+} ions. Thus, the poor electrochemical activity of the latter material correlates to its air stability, as both of these phenomena can be explained by the presence of the passivation Mg oxide on the active mass.

Conclusions

The influence of the crystal structure of surface films on the electrochemical behavior and the chemical stability of intercalation compounds were demonstrated by two examples: (1) possible stabilization of lithium-intercalated graphite electrodes by surface films containing Li_2CO_3 and (2) passivation of HT-synthesized MgCP by MgO surface films.

The high Li-ion conductivity in Li_2CO_3 results from the alternation of the occupied (by Li^+) and empty oxygen tetrahedra, linked by common faces in the crystal structure. The latter serve as transport sites for Li^+ hopping and decrease considerably the energetic barriers of the Li diffusion. In contrast to the graphite case, the co-intercalation of solvent molecules (which solvate Li-ions) into Li_2CO_3 and their transport through Li_2CO_3 crystals are not possible due to the absence of Van-der Waals gaps. Thus, the formation of Li_2CO_3 on the surface of graphite electrodes prevents the co-intercalation of solvent molecules, and consequently, the disintegration of the electrode.

By a combination of synthesis, electrochemistry and XRD analysis, it was shown that in spite of their similarity in structure and composition, Chevrel phase materials obtained by different synthetic routes show a completely different electrochemical activity with magnesium: the full theoretical capacity can be reached with the leached CuCP, while HT-synthesized MgCP reveals

a very poor electrochemical behavior. This unusual phenomenon is caused by the formation of a compact MgO film on the surface of the latter material. The different surface chemistry of the MgCP obtained by different synthetic routes was confirmed by elucidating a correlation between the electrochemical activity and the atmospheric stability of these materials.

Thus, these two examples show that the crystallographic approach is useful, not only for understanding the ionic mobility in the bulk of intercalation compounds, but also for the elucidation of the processes related to the surface of the electrode materials.

Acknowledgments AcknowledgmentsPartial support for this work was obtained from the ISF, Israel Science Foundation and ATU Ltd/Israel. This paper is a part of Ph.D. thesis of E. Lancry in BIU.

References

1. Aurbach D, Markovsky B, Levi MD, Levi E, Schechter A, Moshkovich M, Cohen Y (1999) J Power Sources 81–82:95
2. West AR (1988) Basic solid state chemistry. Wiley, Chichester-New York, p 323
3. Van der Ven A, Ceder G (2000) Electrochem Sol State Lett 3:301
4. Van der Ven A, Ceder G, Asta M, Tepesh PD (2001) Phys Rev B 6418:4307
5. Morgan D, Van der Ven, A, Ceder G (2004) Electrochem Sol State Lett 7:A30
6. Aurbach D, Weissman I, Gofer Y, Levi E (2003) Chem Record 3:61
7. Lancry E, Levi E, Gofer Y, Levi M, Salitra G, Aurbach D (2004) Chem Mater 16:2832
8. Aurbach D, Lu Z, Schechter A, Gofer Y, Gizbar H, Turgeman R, Cohen Y, Moskovich M, Levi E (2000) Nature 407:724
9. Wyckoff RWG (1967) Crystal structures, vol 2. Wiley, New York, p 463
10. Aurbach D (1999) In: Aurbach D (ed) *Nonaqueous electrochemistry*. Marcel Dekker, New York, pp 302–378
11. Markovsky B, Rodkin A, Cohen YS, Palchik O, Levi E, Aurbach D, Kim HJ, Schmidt M (2003) J Power Sources 119–121:504
12. Aurbach D, Gofer Y, Lu Z, Schechter A, Chusid O, Gizbar H, Cohen Y, Ashkenazi V, Moskovich M, Turgeman R, Levi E (2001) J Power Sources 97:28
13. Levi E, Gofer Y, Vestfreed Y, Lancry E, Aurbach D (2002) Chemistry of Materials 14:2767
14. Levi MD, Lancry E, Gizbar H, Lu Z, Levi E, Gofer Y, Aurbach D (2004) J Electrochem Soc 151:A1044
15. Levi MD, Lancry E, Gizbar H, Gofer Y, Levi E, Aurbach D (2004) Electrochim Acta 49:3201
16. Levi MD, Gizbar H, Lancry E, Gofer Y, Levi E, Aurbach D (2004) J Electroanal Chem 569:211
17. Levi MD, Lancry E, Levi E, Gizbar H, Gofer Y, Aurbach D (2005) Sol State Ionics 176:1695
18. Lancry E, Levi E, Gofer Y, Levi M, Aurbach D (2005) J Sol St Electrochem 9:259
19. Yvon K (1979) In: Kaldis E (ed) Current topics in material science, vol 3. Elsevier, North-Holland, pp 53–129
20. Chevrel R, Sergent M, Prigent J (1971) J Sol State Chem 3:515
21. Taniguchi M, Wakihara M, Basu SK (1989) Sol State Ionics 32–33:273